Quantum interference and sharp spin polarization on a double quantum dot: Role of the Rashba spin-orbit interaction

Kuo-Wei Chen,[1,*] Yu-Hsin Su,[1] Son-Hsien Chen,[2] Chien-Liang Chen,[1] and Ching-Ray Chang[1,3,†]

[1]*Department of Physics, National Taiwan University, Taipei 10617, Taiwan*

[2]*Department of Applied Physics and Chemistry, Taipei Municipal University of Education, Taipei 10048, Taiwan*

[3]*Center for Quantum Science and Engineering, National Taiwan University, Taipei 10617, Taiwan*

(Received 6 January 2013; revised manuscript received 30 March 2013; published 29 July 2013)

We analyze the spin-dependent conductance spectrum of a double quantum dot with Rashba spin-orbit and electron-electron interactions based on the Keldysh nonequilibrium Green's function formalism. A clear physical picture emerges from the single-particle analysis of electron-transfer pathways in a quantum dot molecule. It provides an insight into the mechanism that underlies the evolution of bonding resonances. This study demonstrates both numerically and analytically that the mechanism of quantum interference is altered, as either component of the Rashba spin-orbit interaction is modulated. Most importantly, the bonding state can be controlled by tuning the Rashba parameter: a bound state in the continuum becomes unbound upon gate control and vice versa, mediated by the transverse Rashba spin-orbit component. A spin-polarized current is shown to be produced by the interplay of the spin-resolved interference effect with the magnetic flux. Sharp spin polarization that arises from the negative differential conductance, observed over a wide range of values of relevant parameters, is discussed.

DOI: 10.1103/PhysRevB.88.035443 PACS number(s): 73.63.Kv, 72.25.Dc, 71.70.Ej, 85.35.Ds

I. INTRODUCTION

The spin-orbit interaction has become of great interest in recent years because it provides a natural means of controlling the spin.[1] Internal asymmetry, including structure and bulk inversion asymmetries, is responsible for the spin-orbit interaction. Particular attention has been paid to the Rashba spin-orbit (RSO) interaction[2,3] owing to the tunability of its coupling strength via control of the interface electric field by either applying gate voltage or by doping.[4] In devices that use RSO coupling, an effective magnetic field, as a relativistic consequence of the inherent electric field, is coupled to electron spins.[5,6] A precession angle of a moving spin that traverses the Rashba-active region is generated accordingly.[7] Quantum interference of electron spins with various precession angles along various paths is expected and modulated by tuning the RSO coupling strength.[8,9] To control the spin states of electrons that are confined in nanostructures with the RSO interaction is a major challenge in realizing semiconductor spin-based devices, such as spin filter and spin qubits.[10,11]

As well as being a model system for studying the physics of strongly correlated electrons, coupled quantum dots (QDs) are utilized in proposed controllable quantum coherent systems for spintronic devices[12] and quantum information processing.[13] Among various host materials, highly tunable QDs have been realized on top-gate-patterned two-dimensional electron gases in GaAs heterostructures,[14] in which the quantum coherent transport has been demonstrated by the Aharonov-Bohm oscillation[15,16] and Fano effect.[17] The transport characteristics depend strongly on the energy level spacing and the charging energy, and so are governed by the geometry of the QDs. For a coupled double QD (DQD), two conductance peaks smoothly evolve into single Breit-Wigner resonance as the geometry of the system changes from serial to lateral.[18] A molecular state therein with infinite lifetime[19] has been demonstrated to be a bound state in the continuum (BIC), as originally proposed by von Neumann and Wigner.[20] It has been interpreted as being a result of the interference between resonances of different channels.[21] Such resonant states may have applications in quantum computing, owing to the strong reduction of the decoherence processes. As will be established in this study, a BIC can be made well resolved and is fully controllable through the RSO coupling strength. Accordingly, all-electrical control over a particular molecular state, which can be made either open or completely localized, is achievable.

Recently, many efforts have been made to investigate theoretically laterally coupled DQD. Interesting physics such as the Fano-Rashba effect[22] and the Kondo effect[23] have been examined. In particular, the system of interest has been shown to generate a spin-polarized current and its use as a spin filter was further suggested.[24] However, these early studies of electron propagation through lateral DQD with RSO interaction considered only the longitudinal RSO component, rather than the full Rashba Hamiltonian.[25] The RSO effect in these papers is characterized only by spin-dependent phase factors in the tunneling matrix elements, which represent the spin precession in the longitudinal direction, while the laterally propagating electrons do not undergo the RSO interaction. The resulting conductance spectrum is expected simply to exhibit the quantum interference of individual channels which are associated with independent molecular states. The transverse RSO component must also be considered. More complete studies that properly address this subject are therefore required. With respect to a coupled DQD, we argue that wave functions of dot states can penetrate into the tunneling barrier and overlap each other to give a nonzero interdot coupling, which allows the lateral propagation of electrons, so that the RSO component that is associated with the transverse momentum is involved in the spin transport. Meanwhile, nonzero off-diagonal elements emerge; these are calculated from an integral over the product of the wave functions of quasibound states on two dots and the transverse RSO component. Since these off-diagonal elements

correspond to interdot spin-flip coupling, the spin-resolved transport through the lateral DQD is actually more complex than has been considered in the cited studies.

This study begins by briefly discussing the effect of RSO interaction, especially the transverse component, on the spin transport. A closed-form expression for interdot spin-flip coupling is derived based on a comparatively simple potential profile. For simplicity, the analysis focuses on the conditions under which spin-spin interaction[26] and interdot capacitive coupling[27] are negligibly small. Then, the conductance spectrum of laterally coupled DQD with the RSO interaction is presented. Considering the system out of equilibrium under a finite bias, spin-dependent conductance is numerically calculated utilizing the Keldysh Green's function formalism.[28] Missing peaks at the bonding energies, as a result of quantum interference in symmetric DQD with lateral geometry, emerge. As the Rashba parameter increases, the bonding resonances gradually become stronger, indicating that the well-resolved bonding resonances are closely related to the RSO interaction. This fact enables the application of electrical manipulation of the BIC. A physical interpretation is presented and a clear analytical description of the mechanism of the appearance of bonding resonances in the numerical results is provided: the interdot spin-flip coupling that arises from the transverse RSO component is established to have a leading role in modulating the conduction pathways, revealing the BIC. Additionally, the asymmetric phase condition is considered to investigate the effect of the longitudinal RSO component on spin transport in the molecular representation. A simple analytical argument is presented to explain the disappearance of bonding resonances with increasing asymmetry of spin-dependent phases. Furthermore, this study demonstrates that a spin-polarized current is generated as a combined effect of magnetic flux and RSO interaction and, surprisingly, a negative differential conductance is observed. Singular behavior of the spin polarization (SP) follows.

The rest of the paper is organized as follows. Section II describes the model of a lateral DQD. It also presents the derivation of interdot spin-flip coupling strength (Sec. II A) and the self-consistent procedure for obtaining the nonequilibrium Green's functions (NEGF) in the expression for the current (Sec. II B). Section III presents the NEGF calculation of the differential conductance under the weak bias condition as a function of gate voltage (Sec. III A). A clear physical picture and a detailed analysis of the well-resolved bonding resonances are presented (Sec. III B). Then, the spin transport under the asymmetric phase condition is characterized numerically and analytically (Sec. III C). Section IV presents the striking features that are produced when a magnetic flux is applied to the system, and discusses the evolution of the SP and the occupation on the first dot for various gate voltages. Section V draws conclusions. Finally, Appendix A briefly addresses the molecular representation of onsite Coulomb repulsion and Appendix B derives in detail the transmission probability.

II. MODEL

Figure 1 shows a device, whose double-dot structure is formed on a heterostructure that contains a two-dimensional electron gas. Only a single energy level near the Fermi surface

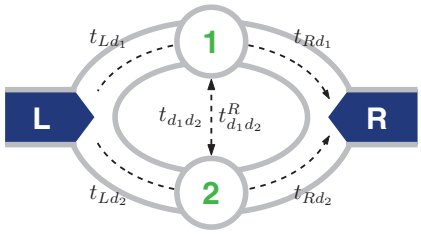

FIG. 1. (Color online) Double quantum dot with Rashba spin-orbit interaction and onsite Coulomb repulsion, coupled laterally to leads denoted as L and R.

is assumed to be relevant to electron transport in each dot because small effective electron mass in a semiconductor results in a large energy separation between single-electron levels. The coupled DQD between two normal metal leads considers both RSO and Coulomb interactions. A longer path for an electron spin to acquire a larger precession angle is realized by considering a locally adjustable Rashba-active path behind the upper dot, forming a Rashba-associated interferometer. The spin transport through individually tunable dot levels under preserved phase coherence is studied here. Experimentally phase-coherent transport through the device under consideration is achievable, and the number of electrons on the dot and the couplings to the leads can be tuned using many gates.[29]

Spin transport through the system is described by the following model Hamiltonian:

$$H = H_0 + H_D + H_{SF} + H_T, \tag{1}$$

where the terms

$$H_0 = \sum_{\alpha=L,R} \sum_{\sigma;k\in L,R} \varepsilon_{\alpha k} n_{\alpha k\sigma} + \sum_{\sigma;j=1,2} (\varepsilon_j n_{j\sigma} + U n_{j\uparrow} n_{j\downarrow}), \tag{2}$$

$$H_D = \sum_{\sigma} t_{d_1d_2} (d^\dagger_{1\sigma} d_{2\sigma} + d^\dagger_{2\sigma} d_{1\sigma}), \tag{3}$$

$$H_{SF} = t^R_{d_1d_2} d^\dagger_{1\downarrow} d_{2\uparrow} - t^{R*}_{d_1d_2} d^\dagger_{1\uparrow} d_{2\downarrow} + t^{R*}_{d_1d_2} d^\dagger_{2\uparrow} d_{1\downarrow} - t^R_{d_1d_2} d^\dagger_{2\downarrow} d_{1\uparrow}, \tag{4}$$

and

$$H_T = \sum_{\sigma;k\in L,R} \sum_{j=1,2} \left(t_{Ld_j} a^\dagger_{Lk\sigma} d_{j\sigma} + t_{Rd_j} e^{-i\sigma\phi_j} a^\dagger_{Rk\sigma} d_{j\sigma} + \text{H.c.}\right) \tag{5}$$

are elucidated as follows. The number operators of electrons on dots and in leads are $n_{j\sigma} = d^\dagger_{j\sigma} d_{j\sigma}$ and $n_{\alpha k\sigma} = a^\dagger_{\alpha k\sigma} a_{\alpha k\sigma}$, respectively, where the fermionic operator $d_{j\sigma}$ ($d^\dagger_{j\sigma}$) destroys (creates) an electron with spin $\sigma = \uparrow, \downarrow$ (or $\sigma = \pm 1$) on the jth ($j = 1,2$) dot, and $a_{\alpha k\sigma}$ ($a^\dagger_{\alpha k\sigma}$) destroys (creates) an electron with energy $\varepsilon_{\alpha k}$ in the lead $\alpha = L, R$.

The first term in Eq. (2) is associated with the leads, which are modeled as a Fermi sea with energy $\varepsilon_{\alpha k}$. Each lead is filled to an electrochemical potential μ_α, and the occupation number obeys the Fermi distribution $f_\alpha(\omega) = \{\exp[(\omega - \mu_\alpha)/k_B T] + 1\}^{-1}$. The second and third terms in

H_0 correspond to the isolated dots. Each dot comprises a single level ε_j and an onsite Coulomb repulsion of constant strength U. Notably, the dot levels are assumed to be spin degenerate because the time-reversal symmetry holds. The RSO interaction originates simply in space inversion symmetry breaking: the state $j\uparrow$ is the time-reversal state of the state $j\downarrow$. The terms H_D and H_{SF} in Eqs. (3) and (4) represent the direct hopping between two dots with coupling strength $t_{d_1d_2}$ and the interdot spin-flip hopping with coupling strength $t^R_{d_1d_2}$, respectively. The last term H_T, given by Eq. (5), is the coupling of the dots to the leads. For simplicity, all elements of the tunneling matrix are assumed to be independent of spin.

A. Effect of Rashba spin-orbit interaction

In Rashba-active regions, spin states are correlated with electron momenta, as described by

$$H_R = \frac{\alpha_R}{\hbar}\hat{y}\cdot(\sigma\times\mathbf{p}) = \frac{\alpha_R}{\hbar}(p_x\sigma_z - p_z\sigma_x). \tag{6}$$

The first term gives rise to energy splitting for electrons of opposite spins and nonzero k_x. Since a bias voltage is applied to the system, electrons are driven to move as dictated by this term, causing the spin precession about the effective magnetic field along the z axis. Then, a spin-dependent phase

$$\sigma\phi = \sigma\frac{\alpha_R m^* L}{\hbar^2} \tag{7}$$

is generated when an electron has traversed a dot,[25] where α_R is the Rashba parameter and L is the length of the dot. As can be seen, an extra one-dimensional pathway behind, say, the first dot can lengthen the spin precession and thereby change the phase accumulation. This fact corresponds to different phase factors that are attached to the tunneling matrix elements in Eq. (5). However, the relationship between the lateral geometry of interest and the second term in Eq. (6) should be highlighted. In addition to moving longitudinally, electrons can transfer laterally from one dot to the other via the direct coupling that arises from overlap between neighboring orbitals. Owing entirely to the finite transverse momentum, the second term is necessarily nonzero and must be carefully considered. Electron spins are therefore subject to the effective magnetic field along the x axis. Clearly, diagonal matrix elements are exactly zero because σ_x flips the spin state to $|\downarrow\rangle$ when it acts on $|\uparrow\rangle$. Meanwhile, nonvanishing off-diagonal elements following the time-reversal invariance represent interdot spin-flip coupling since one relevant energy level in each dot is considered. Briefly, the RSO interaction that is observed from the space-dependent spin coordinate causes the precession of spin in the x direction and spin flip in the z direction. This study will focus on the effect of the RSO interaction on the transport properties and reveal the actual role of each RSO component therein.

Given a potential profile, an explicit expression for interdot spin-flip coupling that helps to specify the real situation in the subsequent numerics is written. It yields more convincing results than can be obtained by making any hand-waving argument. For mathematical simplicity, each dot is modeled as a square potential well. To calculate the corresponding tunneling matrix element, the wave function of each dot is derived separately from the other, and constrained by a condition on the barrier height in an attempt to mimic a DQD that is characterized by the double-well potential. First, for an isolated QD, the eigenfunction is of the form $\psi(x,z) = \sqrt{2/L}\sin n_x\pi x/L\times\psi(z)$. In the transverse direction, the dot is modeled as a semi-infinite well, such that the potential $V(z)$ is

$$V(z) = \begin{cases}\infty, & z\leqslant 0\\ 0, & 0<z<L\\ V_0, & z\geqslant L.\end{cases}$$

For quasibound states, $0\leqslant E<V_0$, the wave functions inside and outside the well are $\psi(z) = A\sin kz$ and $\psi(z) = Ce^{-\kappa(z-L)}$, respectively, with the prefactors $A = (L/2 - \sin 2kL/4k + \sin^2 kL/2\kappa)^{-1/2}$ and $C = A\sin kL$. Then, the following transcendental equation is obtained:

$$\cot kL = -\frac{\kappa}{k} = -\frac{1}{k}\sqrt{\frac{2mV_0}{\hbar^2} - k^2}. \tag{8}$$

An additional condition is imposed on V_0 to ensure that the value of the decaying wave function which penetrates the region of the second dot is reasonably small at $z = 2L + b$; here, $e^{-\kappa(L+b)}\leqslant 0.05$, where b is the width of the tunneling barrier. Therefore, the allowed wave vectors can be numerically determined from Eq. (8). For the other dot, the wave functions of similar form can be easily obtained by the same approach. Owing to the transverse RSO component, the matrix element that represents the interdot spin-flip coupling is given by[25]

$$\langle m\downarrow|u(x)^\dagger\left(-\frac{\alpha_R}{\hbar}p_z\sigma_x\right)u(x)|n\uparrow\rangle \equiv t^R_{mn}, \tag{9}$$

where the unitary operator $u(x) = \exp[-i\sigma_z\int_{x_L}^{x}k_R(x)dx]$ is introduced with $k_R(x) = \alpha_R(x)m^*/\hbar^2$. Substituting the wave functions into Eq. (9) yields

$$t^R_{d_1d_2} = -\frac{2\alpha_R}{\hbar L}\int dx\,\exp[-2ik_R(x-x_L)] \times\sin\frac{m_x\pi x}{L}\sin\frac{n_x\pi x}{L}\times I_z,$$

where the integral of z is

$$\begin{aligned} I_z &= \int dz\,\psi_m^*(z)\left(-i\hbar\frac{\partial}{\partial z}\right)\psi_n(z)\\ &= -i\hbar\kappa ACe^{-\kappa(L+b)}\frac{k + e^{\kappa L}(\kappa\sin kL - k\cos kL)}{\kappa^2+k^2}\\ &\quad - i\hbar\kappa C^2 be^{-\kappa b} - i\hbar kACe^{-\kappa(L+b)}\\ &\quad\times\frac{\kappa - e^{\kappa L}(\kappa\cos kL + k\sin kL)}{\kappa^2+k^2}. \end{aligned}$$

For the ground state, the lowest k and $m_x = n_x = 1$, the spin-flip coupling strength in Eq. (4) is finally obtained as

$$t^R_{d_1d_2} = \alpha_R\frac{iI_z}{\hbar}\frac{\pi^2(1-e^{-2ik_RL})}{2\pi^2k_RL - 2k_R^3L^3}. \tag{10}$$

The coupling strength is straightforwardly identified as a complex number that depends on the DQD geometry and is proportional to the Rashba parameter.

B. Current expression and Green's functions

Now, the employed Keldysh NEGF approach technique is described, before the transport properties of the system are analyzed. The charge current that flows from the left lead into the DQD is derived from the time derivative of the occupation number of conduction electrons in the left lead, which is given by[30]

$$I_\sigma = \frac{2e}{\hbar}\int \frac{d\omega}{2\pi}\,\mathrm{Re}\left[t_{Ld_1}G^<_{d_1L\sigma}(\omega) + t_{Ld_2}G^<_{d_2L\sigma}(\omega)\right], \tag{11}$$

where the lesser Green's function $G^<_{d_jL\sigma}(\omega)$ is the Fourier transform of $G^<_{d_jL\sigma}(t-t') \equiv i\langle\sum_k a^\dagger_{Lk\sigma}(t')d_{j\sigma}(t)\rangle$. The spin-dependent conductance is then defined as $G_\sigma = dI_\sigma/dV$, and the lesser Green's functions therein are related to retarded and advanced Green's functions by assuming that the leads are ideal and applying the kinetic equation

$$\mathbf{G}^< = \mathbf{G}^r\mathbf{g}^{r-1}\mathbf{g}^<\mathbf{g}^{a-1}\mathbf{G}^a, \tag{12}$$

where the boldface terms indicate matrices. The lesser Green's functions for uncoupled systems in Eq. (12) are determined using the fluctuation-dissipation theorem

$$g^<_{\beta\beta\sigma}(\omega) = -f_\beta(\omega)\left[g^r_{\beta\beta\sigma}(\omega) - g^a_{\beta\beta\sigma}(\omega)\right],$$

with $\beta \in L,R,d_1,d_2$, which yields only four nonzero matrix elements $g^{r-1}_{\alpha\alpha\sigma}g^<_{\alpha\alpha\sigma}g^{a-1}_{\alpha\alpha\sigma} = 2if_\alpha(\omega)/\pi\rho$. To obtain the lesser Green's functions, the retarded Green's functions are calculated by applying the Dyson equation

$$\mathbf{G}^r = \mathbf{g}^r + \mathbf{g}^r\Sigma^r\mathbf{G}^r, \tag{13}$$

where the full retarded Green's function in the local basis is a 4×4 matrix

$$\mathbf{G}^r \equiv \begin{pmatrix} G^r_{LL} & G^r_{LR} & G^r_{Ld_1} & G^r_{Ld_2} \\ G^r_{RL} & G^r_{RR} & G^r_{Rd_1} & G^r_{Rd_2} \\ G^r_{d_1L} & G^r_{d_1R} & G^r_{d_1d_1} & G^r_{d_1d_2} \\ G^r_{d_2L} & G^r_{d_2R} & G^r_{d_2d_1} & G^r_{d_2d_2} \end{pmatrix}, \tag{14}$$

and every matrix element in the spin basis is a 2×2 submatrix. The bare Green's functions in the leads under the wide-band approximation are of the form $g^r_\alpha(\omega) = -i\pi\rho$, and $g^r_{d_jd_j\sigma}$ on the dots can be exactly obtained using the equation-of-motion method[31]

$$g^r_{d_jd_j\sigma}(\omega) = \frac{\omega-\varepsilon_j-U+Un_{j-\sigma}}{(\omega-\varepsilon_j)(\omega-\varepsilon_j-U)}, \tag{15}$$

where ρ is the density of states of the leads and $n_{j-\sigma}$ is the occupation number with spin $-\sigma$ on the jth dot. The self-energy, neglecting higher-order terms, is given by the tunneling matrix

$$\Sigma^r \equiv \begin{pmatrix} 0 & 0 & t_{Ld_1} & t_{Ld_2} \\ 0 & 0 & \widetilde{t}_{Rd_1} & \widetilde{t}_{Rd_2} \\ t^*_{Ld_1} & \widetilde{t}^*_{Rd_1} & 0 & \widetilde{t}_{d_1d_2} \\ t^*_{Ld_2} & \widetilde{t}^*_{Rd_2} & \widetilde{t}^*_{d_1d_2} & 0 \end{pmatrix}, \tag{16}$$

with spin-dependent terms

$$\widetilde{t}_{Rd_j} = t_{Rd_j}\begin{pmatrix} e^{-i\phi_j} & 0 \\ 0 & e^{i\phi_j} \end{pmatrix}; \quad \widetilde{t}_{d_1d_2} = \begin{pmatrix} t_{d_1d_2} & -t^{R*}_{d_1d_2} \\ t^R_{d_1d_2} & t_{d_1d_2} \end{pmatrix}. \tag{17}$$

This approximation suffices to study the spin-related phenomena above Kondo temperature[32] such as quantum interference and spin polarization. The occupation number in Eq. (15) is determined self-consistently using the equation

$$n_{j\sigma} = -i\int \frac{d\omega}{2\pi}G^<_{d_jd_j\sigma}(\omega). \tag{18}$$

According to Eqs. (12)–(18), the Green's functions for different spins are correlated with each other not only by the occupation number in bare Green's functions but also by the Dyson equation. Evidently, the spin states of electrons can change when they tunnel between two dots. To determine the convergence, the occupation number (18) on each dot is monitored. Once the lesser Green's functions in the expression for the current (11) have been self-consistently solved, the spin-dependent differential conductance can be calculated.

III. DIFFERENTIAL CONDUCTANCE

Based on the experimental dot-lead coupling strength $\Gamma \approx 0.5$ meV, reasonable values for the parameters in the numerical calculation are settled as follows. The Fermi level is made the origin of energy, and all energies are in units of $\Gamma \equiv 2\pi\rho t^2_{\alpha d_j} \approx 1$ with $\rho = 1$. The Coulomb repulsion strength and the temperature are set to $U = 2$ and $k_BT = 1/\beta = 0.02$, respectively, corresponding to $U = 1$ meV and $T = 116$ mK. A symmetrical chemical potential difference $\mu_L = -\mu_R = V/2$ is used, resulting from a bias voltage $V = 0.02$ that is applied to the leads. The tunneling matrix elements are all simplified to constants $t_{Ld_1} = t_{Rd_1} = t_{Ld_2} = t_{Rd_2} = 0.4$ and the direct coupling strength $t_{d_1d_2} = 0.8$. The Rashba parameter is assumed to be $\alpha_R \approx 0.3$ eV Å, which determines the precession angle $\phi = 1.3687$ and the spin-flip coupling strength $t^R_{d_1d_2} \approx 0.4\exp(0.2021)$, if the dot size $L = 70$ nm and the barrier width $b = 35$ nm. For an extended Rashba-active path, considered in Sec. III C, one spin-dependent phase is set independently of the other, corresponding to the local tunability.

In the Introduction, the transport of electrons through a noninteracting symmetric DQD with lateral geometry was mentioned. That only the antibonding state is well resolved in the conductance curve has been shown.[18] Accordingly, the bonding state is fully decoupled from the leads and becomes localized in the conduction band. The following focuses on the effects of RSO and Coulomb interactions on spin transport through a lateral DQD under weak bias. The above-mentioned BIC phenomenon certainly serves as the limiting case of a zero Rashba parameter, and shall be reconfirmed by both numerical calculation and analytical argument. In particular, the bonding and antibonding states are demonstrated to be bridged in the presence of the transverse RSO component.

A. Well-resolved bonding resonances

Figure 2(a) presents the conductance as a function of individual dot levels ε_1 and ε_2 for RSO coupling strength $\phi_1 = \phi_2 = 1.3687$, which is symmetric about the off-diagonal line because of the symmetry between ε_1 and ε_2 in the Hamiltonian (1). The RSO interaction strongly affects the total conductance, including the phases and positions of the resonances and antiresonances. In particular, four resonant peaks are observed in the off-diagonal direction. These correspond to two pairs

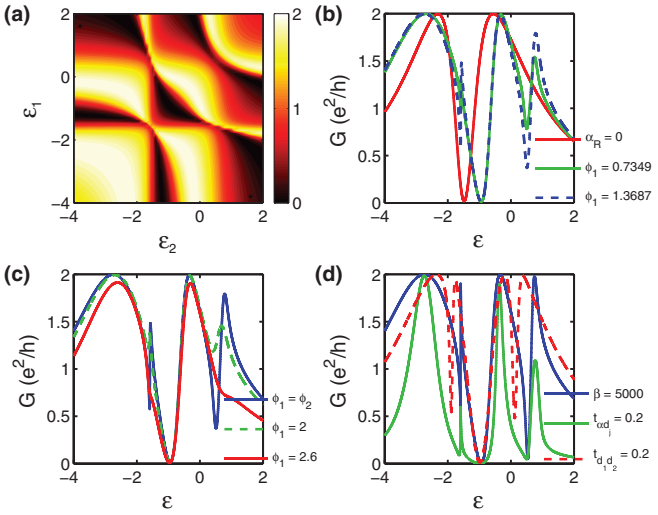

FIG. 2. (Color online) Consider $V = 0.02$, $U = 2$, and $k_BT = 0.02$. (a) Conductance spectrum for $\phi_1 = \phi_2 = 1.3687$. Differential conductance with $\varepsilon_1 = \varepsilon_2 \equiv \varepsilon$ for (b) $\phi_1 = \phi_2$, (c) fixed $\phi_2 = 1.3687$, and (d) $\phi_1 = \phi_2 = 1.3687$. Corresponding $t^R_{d_1d_2} = 0.4 \exp(0.2021)$ in (a), (c), and (d).

of bonding and antibonding resonances. By comparison with the BIC phenomenon that was identified in the aforementioned study, clearly, the emergence of the bonding resonances herein is attributed to the RSO interaction. To confirm this association, the case of zero interdot level detuning $\varepsilon_1 = \varepsilon_2 \equiv \varepsilon$ for three Rashba parameter strengths $\alpha = 0$, 0.16, and 0.298 eV Å, as presented in Fig. 2(b), is considered. In the absence of the RSO interaction, two peaks to the left of $\varepsilon = 0$ and $-U$ are observed. Each Coulomb peak is known to split into two, which are associated with the bonding and antibonding states, owing to the overlap of the wave functions and the spin degeneracy that is lifted by the Pauli exclusion principle, if phase-coherent tunneling occurs between the two dots.[33] For $\alpha_R = 0$, numerical calculation of the differential conductance that exhibits two peaks, separated by a Coulomb gap, confirms that only the antibonding state is involved in electron conduction. As the Rashba parameter increases, another two peaks to the right of $\varepsilon = 0$, $-U$ emerge, and conductance returns to having the normal four-peaked profile. This crossover exactly shows the bound-unbound transition in which the BIC is gradually revealed. As a result of the coupling of the state to electron reservoirs, the finite lifetime of the bonding state is manifested in peak broadening. To gain insight into the importance of the RSO interaction in this transition and to study further the origin of the implied bridging effect that causes the appearance of bonding resonances, the Hamiltonian is now analyzed to identify the actual electron-transfer pathways.

B. Role of transverse Rashba spin-orbit coupling

To present a clear physical interpretation of spin transport through a DQD, the Hamiltonian, in which the molecular operators are used, is rewritten by applying the following rotation:

$$\begin{pmatrix} d_{B\sigma} \\ d_{A\sigma} \end{pmatrix} = \begin{pmatrix} \cos\theta & -\sin\theta \\ \sin\theta & \cos\theta \end{pmatrix} \begin{pmatrix} d_{1\sigma} \\ d_{2\sigma} \end{pmatrix},$$

where $d_{B\sigma}$ and $d_{A\sigma}$ are annihilation operators of the bonding and antibonding states with spin σ, respectively. Consider the case $\varepsilon_1 = \varepsilon_2 \equiv \varepsilon$; the angle of rotation is defined as $\theta = \pi/4$. The inverse transformation is

$$\begin{pmatrix} d_{1\sigma} \\ d_{2\sigma} \end{pmatrix} = \frac{1}{\sqrt{2}} \begin{pmatrix} d_{B\sigma} + d_{A\sigma} \\ -d_{B\sigma} + d_{A\sigma} \end{pmatrix}. \tag{19}$$

A coupled DQD in the absence of the Coulomb interaction is considered first. Substituting Eq. (19) into single-particle terms in the Hamiltonian (1) yields

$$H_N = \sum_\sigma \left(\varepsilon n_{1\sigma} + \varepsilon n_{2\sigma} + t_{d_1d_2} d^\dagger_{1\sigma} d_{2\sigma} + t_{d_1d_2} d^\dagger_{2\sigma} d_{1\sigma}\right) = \sum_\sigma \left[\left(\varepsilon - t_{d_1d_2}\right) d^\dagger_{B\sigma} d_{B\sigma} + \left(\varepsilon + t_{d_1d_2}\right) d^\dagger_{A\sigma} d_{A\sigma}\right], \tag{20}$$

$$H_{SF} = t^R_{d_1d_2} d^\dagger_{1\downarrow} d_{2\uparrow} - t^{R*}_{d_1d_2} d^\dagger_{1\uparrow} d_{2\downarrow} + t^{R*}_{d_1d_2} d^\dagger_{2\uparrow} d_{1\downarrow} - t^R_{d_1d_2} d^\dagger_{2\downarrow} d_{1\uparrow} = t^R_{d_1d_2} d^\dagger_{B\downarrow} d_{A\uparrow} - t^{R*}_{d_1d_2} d^\dagger_{B\uparrow} d_{A\downarrow} + t^{R*}_{d_1d_2} d^\dagger_{A\uparrow} d_{B\downarrow} - t^R_{d_1d_2} d^\dagger_{A\downarrow} d_{B\uparrow}, \tag{21}$$

$$\begin{aligned} H_T &= \sum_{\sigma;k\in L,R} \sum_{j=1,2} \left(t_{Ld_j} a^\dagger_{Lk\sigma} d_{j\sigma} + t_{Rd_j} e^{-i\sigma\phi_j} a^\dagger_{Rk\sigma} d_{j\sigma} + t^*_{Ld_j} d^\dagger_{j\sigma} a_{Lk\sigma} + t^*_{Rd_j} e^{i\sigma\phi_j} d^\dagger_{j\sigma} a_{Rk\sigma}\right) \\ &= \sum_{\sigma;k\in L,R} \sum_{j=B,A} \left(t_{Ld_j} a^\dagger_{Lk\sigma} d_{j\sigma} + t_{Rd_j\sigma} a^\dagger_{Rk\sigma} d_{j\sigma} + t^*_{Ld_j} d^\dagger_{j\sigma} a_{Lk\sigma} + t^*_{Rd_j\sigma} d^\dagger_{j\sigma} a_{Rk\sigma}\right), \end{aligned} \tag{22}$$

where the effective tunneling matrix elements are defined as

$$t_{Ld_B} = \frac{1}{\sqrt{2}} t_{Ld_1} - \frac{1}{\sqrt{2}} t_{Ld_2}, \quad t_{Ld_A} = \frac{1}{\sqrt{2}} t_{Ld_1} + \frac{1}{\sqrt{2}} t_{Ld_2} \tag{23}$$

and

$$\begin{aligned} t_{Rd_B\sigma} &= \frac{1}{\sqrt{2}} t_{Rd_1} e^{-i\sigma\phi_1} - \frac{1}{\sqrt{2}} t_{Rd_2} e^{-i\sigma\phi_2}, \\ t_{Rd_A\sigma} &= \frac{1}{\sqrt{2}} t_{Rd_1} e^{-i\sigma\phi_1} + \frac{1}{\sqrt{2}} t_{Rd_2} e^{-i\sigma\phi_2}. \end{aligned} \tag{24}$$

Notably, Eq. (20) shows that two coupled dots effectively are treated as a single dot with two energy levels in its molecular representation. Nevertheless, H_{SF} and H_T maintain the same form as before the rotation, as seen in the one-to-one correspondence between two bases. The redefinition, in which the rotation of the tunneling matrix elements is equivalent to that of the bare QD operators, yields the tunneling Hamiltonian (22) that describes the couplings of molecular states to two leads. In particular, Eqs. (23) and (24) clearly describe the BIC that is formed in a totally symmetric DQD with lateral geometry. For

$t_{\alpha d_1} = t_{\alpha d_2}$ and $\phi_1 = \phi_2, t_{Ld_B} = t_{Rd_B\sigma} = 0$. Therefore, only the antibonding state is coupled to the reservoirs. Lastly, and most importantly, one of the key effects of the RSO interaction is emphasized. Clearly, the interdot spin-flip coupling (4) in the original Hamiltonian appears to provide a means of electron transfer between two dots as an alternative to the direct coupling (3). The picture, however, changes when the current representation of the system is considered. The direct coupling strength is absorbed into the renormalized bare dot level, while the form of H_{SF} remains the same. In fact, as indicated by Eq. (21), the interdot spin-flip coupling acts as an intermolecular-level coupling. The physics of spin transport in the system under consideration, for example the BIC phenomenon, is thus expected to be altered greatly if the bonding and antibonding states are coupled to each other. When the transverse RSO component is not considered, the antibonding state alone governs electron transport. Additionally, the analysis of spin-resolved transport that is based on Eqs. (23) and (24) can also be applied to other geometries, such as that of a serially coupled DQD embedded in a ring.[34] The serial DQD is expressed as two independent pathways that are exactly antiphase with each other. Phases of electron wave functions along the two pathways change simultaneously as the spin-dependent phases increase, which effect is reflected in the evolution of the phases in the bonding and antibonding resonances. The Fano antiresonances are understood to be caused by interference between either molecular and continuum states.

In summary, in the coherent transport regime, a coupled DQD can be expressed in terms of nondegenerate molecular states. The energy levels and their spacing are set by the magnitude of zero-detuning energy level ε and the strength of interdot direct coupling $t_{d_1d_2}$. Considering symmetric configuration then leads to localization of the bonding state. The transverse RSO component, however, establishes a coupling between molecular states. Through the coupling electrons can reach the bonding state with their spins flipped. Therefore, the bonding state ceases to be isolated, but becomes indirectly coupled to the conduction electrons via the antibonding state. This physical picture that emerges from the single-particle analysis provides a basic and qualitative understanding of the considered system, and can be used to elucidate the physics of the evolution of the bonding resonances that is observed in the NEGF results obtained herein. Appendix A briefly addresses the transformation of onsite Coulomb repulsion.

The laterally coupled DQD is now mapped onto a single QD molecule (SQDM). Consider $\alpha_R = 0$, as presented in Fig. 2(b). The missing bonding resonances have already been explained with reference to Eqs. (23) and (24). The bonding state that is fully decoupled from both leads and the antibonding state becomes a BIC because of interference and zero intermolecular-level coupling. As the Rashba parameter increases, the magnitudes of the spin-dependent phases and the interdot spin-flip coupling simultaneously vary, as described by Eqs. (7) and (10), respectively. The spin-dependent phase factors in the dot-lead matrix elements, which result in a phase evolution in transported electrons through molecular states,[34,35] are basically complex numbers between positive and negative unity for both up- and down-spin electrons. The bonding resonances gradually become well resolved as the magnitude of the strength of spin-flip coupling increases. Here, the coupling strengths are $0, 0.23\exp(0.8359)$, and $0.4\exp(0.2021)$, indicating that an increasing number of electrons propagate through the bonding state. Resonant tunneling is known to occur simply when a molecular level is aligned with either of the leads. When the bonding state is uncoupled from both leads, the emerging bonding resonances suggest the conduction pathway in which electrons can propagate through the bonding state via the antibonding state. Additionally, the conductance peaks to the right of $\varepsilon = 0, -U$ behave similarly. This phenomenon shows that the mechanism by which electrons overcome the Coulomb repulsion to propagate through the bonding state, as associated with the higher effective energy level that is also decoupled from both leads, is the same as the mechanism of electron transport through an empty bonding state, in the framework of the NEGF formalism to a first-order approximation of the self-energy (16). Because the conductance peaks to the left of $\varepsilon = 0, -U$ are maximal, the pathway through the antibonding state is characterized by a fully open channel as a result of direct connections to the leads.

Since the bonding state is proved to be entirely uncoupled from the two leads, the well-resolved bonding resonances are attributed to indirect coupling between the bonding state and the leads via the antibonding state. Accordingly, electrons from the left lead transfer between molecular states through interlevel spin-flip coupling (21), before finally leaving the antibonding state to the right. This process exposes the bonding state to electron reservoirs and is demonstrated by the conductance. In this interpretation, electrons are assumed to overcome the initial energy difference between the Fermi level of the left lead and the antibonding level to arrive at the bonding level, such that the transmission probability is reduced by the level spacing, which effect is actually seen in the suppression of the peaks. To confirm this claim, the differential conductance for a smaller direct coupling strength $t_{d_1d_2} = 0.2$ than considered in Fig. 2(b), with the other parameters unchanged, is calculated, yielding the results that are presented in Fig. 2(d). The peak values of the bonding resonances clearly increase and almost reach their maxima. The direct coupling in the molecular representation is demonstrated to be responsible for the level spacing. Reducing the strength of direct coupling therefore reduces the initial energy difference that electrons must overcome, increasing the probability of electron conduction through the bonding state. Accordingly, an increase in conductance is expected. A clear physical basis for the characteristics that are observed in Fig. 2(b) has therefore been established both numerically and analytically. In particular, as the transverse RSO component is modulated, the quantum interference varies with the electron-transfer pathways. The interference is initially that which causes the formation of BIC. It becomes the interference of resonances that are associated with different pathways through molecular states, as evident in the appearance of Fano resonances. Most importantly, the BIC is demonstrated to be controllable by tuning the Rashba parameter. Previously, the BIC had been shown to be controllable only by applying a magnetic field.[36] Here, all-electrical control over the bonding state to make it either

open or completely localized, mediated by the transverse RSO component, is achievable.

At this point, some characteristics of conductance are briefly discussed with reference to the case with $\phi_1 = 1.3687$ in Fig. 2(b). Above, the symmetric DQD with lateral geometry is mapped onto a T-shaped SQDM. Interference between electrons that move along two paths with different linewidths leads to a resonant scattering phenomenon, called Fano resonance. The asymmetric line shape and the resonant destructive interference, not clearly visible in Fig. 2(b), are much more noticeable in Fig. 2(d), in which the weak coupling is considered. With respect to the bonding and antibonding energies, the presented physical interpretation has the purpose of clarifying the involvement of the transverse RSO component in spin transport and the conductance behavior. In the case in which the Hamiltonian of a laterally coupled DQD, excluding the Coulomb interaction, is diagonalized the eigenvalues for a SQDM are related to both direct and spin-flip coupling strengths. In Appendix B, single-particle transmission is derived as a basis for the analytical description of both Fano resonance and level renormalization, mentioned above. Figure 2(d) presents the effects of temperature. As the temperature falls, the conductance profile remains qualitatively unchanged, whereas certain characteristics become stronger at lower temperature: the bonding resonances become stronger and the Fano antiresonances become deeper. The motion of electrons in the system of interest has now been elucidated. Lastly, the phase behavior of electrons that are traversing the SQDM along two pathways is addressed. The phase remains when an electron with either spin hops from the left lead to the antibonding state. In the subsequent hopping to the right, the up-spin electron acquires a phase $-\phi$ while the down-spin electron acquires a phase ϕ. An electron that travels between molecular states acquires no phase other than π, due to spin flips. In conclusion, the phase difference between electrons with a particular spin that pass through bonding and antibonding states, aside from that which arises from Fano resonance, originates in the spin-flip contributions to the wave function. The spin-dependent phases then dominate the difference between spins. To study further the effect of the longitudinal RSO component, the phase values are changed and the effect on the spin transport is discussed.

C. Role of longitudinal Rashba spin-orbit coupling

A two-path interferometer that considers different spin precession angles along the two paths is proposed. This interferometer can be realized by lengthening the one-dimensional Rashba-active path between one QD and the right lead to form an extended path, or the Rashba parameter of that lengthened path is locally adjustable. This interferometer is used herein to investigate the interference phenomenon that is associated with asymmetric spin-dependent phases. The system without interdot couplings is the simplest Rashba spin interferometer. The interference of electrons is modified by tuning the Rashba parameter of one of the paths, and the conductance is expected to oscillate upon such tuning. However, the mechanism of interference is more complex for a coupled DQD. Figure 2(c) plots differential conductance versus zero-detuning energy level ε for various spin-dependent phases $\phi_1 = 1.3687, 2, 2.6$. As the phase ϕ_1 is tuned, only antibonding resonances are maintained and the corresponding values are slightly changed. In contrast, the peak values of the bonding resonances are gradually reduced, until they disappear. This phenomenon is expected to be associated with the interference. Further insight into the physics that underlies these results is gained by examining the effect of the phase change on conduction pathways.

Altering the value of ϕ_1 effectively modifies the couplings of the molecular states to the two leads. In the model herein, the couplings between molecular states and the left lead are independent of both RSO coupling and spin, and they remain fixed at $t_{Ld_B} = 0$ and $t_{Ld_A} = 0.57$, as indicated by Eq. (23). With respect to the couplings between molecular states and the right lead, in the symmetric case $\phi_1 = \phi_2$, $t_{Rd_B\sigma}$ remains zero, while $t_{Rd_A\sigma} = 0.11 \mp 0.55i$ for up and down spins, respectively. This configuration is that presented in Figs. 2(a) and 2(b), and the acquired phases that correspond to different spins oppose each other but the real parts of the coupling strengths are the same. In the asymmetric case that is described by Eq. (24), the coupling $t_{Rd_B\sigma}$ ceases to be zero when $\phi_1 \neq \phi_2$. Basically, $t_{Rd_B\sigma}$ and $t_{Rd_A\sigma}$ oscillate with ϕ_1 with a period of 2π. Unlike in the preceding case, the coupling $t_{Rd_B\sigma}$ is not suppressed, and electrons in the bonding state can exit that state in two ways: either by directly hopping onto the right lead or via the antibonding state.

A single-particle description of the system is proposed here. When the bonding level is aligned with the Fermi level of the left lead, the wave function of an incident unpolarized electron is given using the eigenbasis of S_z by $\Psi^{\text{in}} = A\psi_\uparrow + B\psi_\downarrow$. The outgoing wave function is of the form $\Psi^{\text{out}} = C\psi_\uparrow^{(B)} + D\psi_\uparrow^{(A)} + E\psi_\downarrow^{(B)} + F\psi_\downarrow^{(A)}$, which takes into account all of the transport pathways and spins. Quantum interference arises between coherent waves with similar amplitudes and different phases. More tunneling events correspond to the weaker effective coupling strength. Therefore, the leading terms that are associated with the bonding state correspond to the direct pathway along which an electron in the bonding state is transferred directly to the right lead. For the first-order tunneling process, the effective coupling strength between two leads in the direct pathway is

$$\begin{aligned} T_{LR}^{(B)} &= |t_\uparrow + t_\downarrow|^2 = \left| t_{Rd_B\downarrow} t_{d_1d_2}^R t_{Ld_A} + t_{Rd_B\uparrow} \left(-t_{d_1d_2}^{R*}\right) t_{Ld_A} \right|^2 \\ &= 2 \left| t_{Rd_B\sigma} \right|^2 \left| t_{d_1d_2}^R \right|^2 t_{Ld_A}^2 \left(1 - \cos 2\phi_{RB}\right), \end{aligned} \tag{25}$$

where $\phi_{RB} = \arg\left(t_{d_1d_2}^R t_{Rd_B\downarrow}\right)$. Evidently, Eq. (25) indicates that the destructive interference can occur between electron wave functions through the same pathway for different spins when $\phi_{RB} = 0$, meaning that the argument of $t_{Rd_B\downarrow}$ compensates for that of $t_{d_1d_2}^R$.

In Fig. 2(c), the phase of $t_{d_1d_2}^R$ remains 0.2. Equation (24) indicates that, as the phase ϕ_1 is tuned from 1.3687 to 2, the phase of $t_{Rd_B\downarrow}$ transiently increases above zero and then falls to -0.02; this effect is responsible for the reduction of conductance in numerical calculation. Additionally, the effective coupling strength (25) enables the transmission probability to be suppressed to zero as the phase of $t_{Rd_B\downarrow}$ approaches -0.2, analytically corresponding to $\phi_1 = 2.87$

[Eq. (24)]. The vanishing of the bonding resonances from the conductance curve at $\phi_1 = 2.6$, corresponding to $\arg(t_{Rd_B\downarrow}) = -0.13$ [Eq. (24)], verifies the above explanation and shows that the destructive interference can occur before the predicted exact cancellation of the two phases; this phenomenon may be relevant to the many-body correlations. Evidently, the conductance around bonding energies returns almost to the background that arises from the tails of the antibonding resonances. Therefore, the numerical conductance behavior can be qualitatively described by the analytical argument concerning the interference effect, and the role of the longitudinal RSO component in the evolution of bonding resonances is demonstrated. The electrical manipulation of the spin-dependent phase effectively alters the couplings between molecular states and leads, and influences the spin-resolved electron transport. Additionally, the Fano antiresonances are eliminated, implying that the destructive interference between electrons through bonding and antibonding states is greatly weakened. In place of the interference along two pathways through the T-shaped SQDM, the interference is now that of spins along a single pathway as the spin-dependent phase is varied. With regard to the antibonding resonances, the phase change hardly affects conductance because of the direct access of that state to both leads.

IV. SPIN POLARIZATION

The configuration of propagation pathways across the SQDM depends nonmonotonically on the RSO interaction, which is primarily characterized by the evolution of conductance peaks. Most importantly, the preceding section presented a clear physical picture of the spin-resolved electron transport through a lateral DQD, which emerged from the single-particle analysis, providing a simple and qualitative understanding of the bound-unbound transition and quantum interference. However, the current that passes through the device remains unpolarized. To achieve this critical goal of spintronics, an earlier study demonstrated that both the magnitude and the direction of the induced spin-polarized current in an Aharonov-Bohm ring with serially coupled DQD can be controlled by varying the gate voltage, RSO coupling strength, or magnetic flux strength.[37] Here, the conditions for generating spin-polarized current and spin transport through the considered Rashba interferometer under magnetic flux are studied.

A vector potential $\mathbf{A}$ gives rise to a phase factor that is attached to the transition amplitude of the electrons that propagate along paths that enclose the magnetic flux. The phase factor in the tunneling matrix elements captures the effect of the magnetic flux. The other terms are thus unchanged, and the revised tunneling Hamiltonian is

$$H_T = \sum_{\sigma;k\in L,R} \big(t_{Ld_1} e^{i\phi_M/2} a^\dagger_{Lk\sigma} d_{1\sigma} + t_{Ld_2} e^{-i\phi_M/2} a^\dagger_{Lk\sigma} d_{2\sigma} + t_{Rd_1} e^{-i\phi_M/2} e^{-i\sigma\phi_1} a^\dagger_{Rk\sigma} d_{1\sigma} + t_{Rd_2} e^{i\phi_M/2} e^{-i\sigma\phi_2} \times a^\dagger_{Rk\sigma} d_{2\sigma} + \text{H.c.}\big).$$

In the NEGF formalism, the self-energy matrix incorporates the spin-independent phase $\phi_M = 2\pi\Phi/\Phi_0$, where Φ is the magnetic flux that is enclosed by each subcircuit and $\Phi_0 = hc/e$ is the magnetic flux quantum. With respect to the physical interpretation that is presented in Sec. III B, the phase factors are clearly incorporated into the effective tunneling matrix elements. Notably, the magnetic flux is involved in the couplings between molecular states and two leads, so the magnetic flux can be controlled to manipulate the configuration of the propagation pathways. Indeed, this approach is the conventional approach for controlling the BIC in the absence of the RSO interaction.

Figure 3(a) plots the spin-dependent conductance as a function of zero-detuning energy level ε for asymmetric spin-dependent phases with magnetic flux strength $\phi_M = \pi/4$. The well-separated curves for the up and down electron spins verify that a spin-polarized current is generated. In contrast, for symmetric phases, the curves overlap. These results reveal that a laterally coupled DQD can act as a spin current generator only under both phase asymmetry and a magnetic flux. In particular, the differential conductance for the up-spin electrons is, surprisingly, negative in some areas. This characteristic is associated with a special phenomenon, which is presented in Fig. 3(b) by plotting the spin polarization (SP) of differential conductance, defined as $\eta \equiv (G_\uparrow - G_\downarrow)/(G_\uparrow + G_\downarrow)$. Under the symmetric phase condition, $\phi_1 = \phi_2$, the SP is always zero; this phenomenon indicates that the origin of the spin-polarized current lies in the interplay of combined effect of magnetic flux and RSO interaction. As ϕ_1 deviates from ϕ_2, a finite SP fluctuates with ε. At particular energies, the SP is observed to change dramatically, as exemplified by the curve of $\phi_1 = 2$. The SP can reach several thousands, and reverses sharply. Such

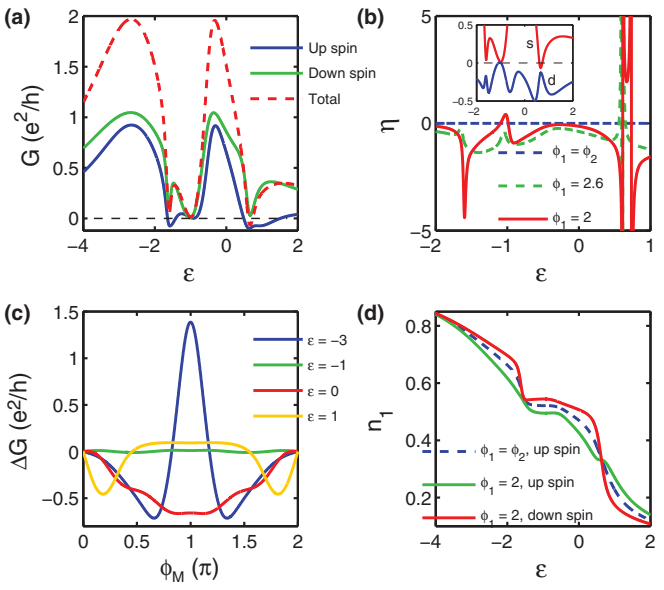

FIG. 3. (Color online) Consider $V = 0.02$, $U = 2$, $k_BT = 0.02$, $t^R_{d_1d_2} = 0.4\exp(0.2021)$, and fixed $\phi_2 = 1.3687$. (a) Differential conductance with $\varepsilon_1 = \varepsilon_2 \equiv \varepsilon$ for $\phi_1 = 2$ and $\phi_M = \pi/4$. (b) Spin polarization for $\phi_M = \pi/4$, and the sum and difference of spin-dependent conductance in (a), denoted as s and d, respectively, plotted in the inset. (c) Conductance difference $G_\uparrow - G_\downarrow$ for $\phi_1 = 2$. (d) Electron occupation on the first dot for $\phi_M = \pi/4$. Dashed lines in (a) and inset in (b) indicate the zero conductance.

a strong SP does not arise from a fully spin-polarized current. In fact, this remarkable phenomenon is related to the negative differential conductance and the resultant singularity. The dashed line in Fig. 3(a) indicates zero conductance. The output current is expected to be down-spin polarized whenever the up-spin conductance curve intersects the dashed line. Even so, the SP under this special condition is -1. The only cause of the strong SP is therefore the exact cancellation of $G_\uparrow$ by $G_\downarrow$ in the denominator of the definition of SP. The inset in Fig. 3(b) plots the sum of, and the difference between, the spin-dependent conductances. The difference is mostly below zero. The positive sum therefore yields a negative SP at most energies. Also, the zero in the denominator is expected whenever the sum intersects the dashed line, yielding an infinite SP. According to the definition, SP has opposite signs on opposite sides of the crossing points, and is not well defined at the points. Accordingly, two sharp reversals of SP close to the crossing points are observed. Singular behavior, including the strong SP and the sharp reversal, are therefore demonstrated to originate from the negative differential conductance in the considered device. Additionally, the magnitude of SP is normally between zero and one. In the region of negative differential conductance, however, the magnitude can exceed unity.

The change in the direction of SP as the applied magnetic flux is tuned is considered. The difference in the conductance between the spins, presented in Fig. 3(c) and denoted as $\triangle G = G_\uparrow - G_\downarrow$, varies with the magnetic phase ϕ_M, and the curves for various ε exhibit distinct behaviors. Clearly, the output current can be either up- or down-spin polarized. At the symmetric point $\varepsilon = -1$, the magnetic flux has almost no effect on the curve. However, the curve is below zero for $\varepsilon = 0$. The magnitude of the corresponding negative SP exceeds one as the up-spin conductance becomes negative. Also, the SP exhibits a singularity as it passes through the point $\phi_M = \pi$, where it changes sign. In particular, the curve for $\varepsilon = -3$ oscillates with ϕ_M and exceeds one because the oscillatory conductance for different spins is almost symmetric about the zero line. The figure does not show the spin-dependent conductance. Although the current is demonstrated to be spin polarized, the spin accumulation on the DQD does not necessarily arise from the steady-state spin-polarized current, as will be elucidated below.

Figure 3(d) plots the electron occupation on the first dot as a function of zero-detuning energy level ε at magnetic flux strength $\phi_M = \pi/4$ under both symmetric and asymmetric phase conditions. The overlapping of curves for up and down spins reveals that no spin accumulation is induced at $\phi_1 = \phi_2$. For asymmetric phases, the different curves for up- and down-spin electrons verify the existence of a spin-polarized dot. Restated, magnetic flux in combination with Rashba-associated quantum interference suffices to induce the spin-polarized occupation under the weak bias condition. The behavior of n_1 exhibits a complex dependence on ε. Both gradual and sharp drops as well as charge oscillation are observed in the curves, and the electron transfer process is expected to deviate greatly from that associated with the standard Coulomb blockade. n_2 exhibits the same behavior. Furthermore, the energies at which the differential conductance is negative and the down-spin electron occupation drops to approach, and cross, the up-spin electron occupation are close to the bonding energies, as obtained from Figs. 3(a), 3(d) and 2(c). This fact suggests that the mechanism that is responsible for the negative differential conductance and the fluctuation in n_1 may be associated with the bonding state, such as, for example, a change in electron-transfer pathways through the bonding state. Finally, a comparison of Fig. 3(a) with Fig. 3(d) exhibits that the output current remains down-spin polarized and negative spin accumulation lasts until $\varepsilon = 0.63$ at which it becomes positive. No explicit correlation between spin accumulation and spin-polarized current is thus demonstrated.

V. CONCLUSION

Spin transport through a laterally coupled DQD was studied considering the RSO interaction and onsite Coulomb repulsion. Efforts were made to characterize quantum interference and spin polarization both numerically and analytically. Numerically, a bias voltage across the DQD is considered, and spin-dependent conductance within the framework of the Keldysh NEGF technique is calculated, and the nonequilibrium situation and many-body correlations are incorporated. The reasonable values for parameters of interest make the predicted characteristics experimentally observable. A simple elucidation of the transport characteristics that are observed in our NEGF results is provided using an analytical approach. When the deformation that arises from many-body effects is excluded, the main features of the evolution of bonding resonances can be qualitatively explained by single-particle analysis.

Because of the lateral propagation of electrons, off-diagonal elements of RSO interaction should be nonvanishing, even in the case that only a single energy level in each dot is relevant to electron transport. The complete effect of the RSO interaction, including the spin-dependent phase and spin-flip coupling, is considered, and a closed-form expression for the interdot spin-flip coupling is derived. Bonding resonances are numerically shown to become well resolved. Therefore, a BIC that is revealed by the RSO interaction becomes unbound. To provide an insight into the underlying mechanism, a clear physical picture, which emerges from the single-particle analysis of electron-transfer pathways, is presented. A symmetric DQD with lateral geometry can be mapped onto a T-shaped SQDM with antibonding state coupled to two leads only. The direct coupling then determines the level spacing, and the interdot spin-flip coupling is interpreted as an intermolecular-level coupling. The level-lead matrix elements depend on the spin-dependent phases. The mechanism of quantum interference, varying with the electron-transfer pathways as either component in the RSO interaction is modulated, is altered in two ways. First, in the presence of spin-flip coupling, the bonding state is exposed to electron reservoirs via the antibonding state, such that the interference phenomenon, which is originally the interference that results in the BIC, becomes the interference of resonances on different pathways through molecular states, as reflected by the appearance of Fano resonances. In such a case, the importance of the transverse RSO component is manifested chiefly in the fact that the BIC can be electrically controlled by tuning the

Rashba parameter to be either open or completely localized. However, with respect to the effect of the longitudinal RSO component, the mechanism of the aforementioned interference between electrons along the two pathways through the T-shaped SQDM is further altered as one of the spin-dependent phases is varied. Electrons now have two ways to leave the bonding state, and the interference of spins along a single pathway is dominant. This evolving interference phenomenon is explained by an analytical argument concerning the effective coupling strength that yields destructive interference, as evidenced by the suppressed peaks and the elimination of Fano antiresonances in the numerical result. In both cases, electrons must overcome the spacing between molecular levels, and this requirement is numerically examined. Therefore, a remarkable change in transport characteristics with the modulation of RSO interaction is essentially related to the rearrangement of electron-transfer pathways through the SQDM. Furthermore, the generation of a spin-polarized current is demonstrated to require both magnetic flux and phase asymmetry. Negative differential conductance is observed; it results in the strong SP and sharp reversal, by the conventional definition. The analysis herein suggests that the mechanism that is responsible for the negative differential conductance and the fluctuation in occupation may be associated with the bonding state.

ACKNOWLEDGMENT

The authors would like to thank the National Science Council of the Republic of China, Taiwan, for financially supporting this research under Contract No. NSC101-2112-M-002-011-MY3.

APPENDIX A

The two-particle terms in the Hamiltonian (2) under transformation are

$$\begin{aligned} H^M &= Un_{1\uparrow}n_{1\downarrow} + Un_{2\uparrow}n_{2\downarrow} \\ &= \frac{U}{2}(n_{B\uparrow}n_{B\downarrow} + n_{A\uparrow}n_{A\downarrow} + n_{B\uparrow}n_{A\downarrow} + n_{A\uparrow}n_{B\downarrow}) \\ &\quad + \frac{U}{2}(-d^\dagger_{B\uparrow}d^\dagger_{B\downarrow}d_{A\uparrow}d_{A\downarrow} - d^\dagger_{A\uparrow}d^\dagger_{A\downarrow}d_{B\uparrow}d_{B\downarrow}) \\ &\quad + \frac{U}{2}(d^\dagger_{B\uparrow}d^\dagger_{A\downarrow}d_{B\downarrow}d_{A\uparrow} + d^\dagger_{B\downarrow}d^\dagger_{A\uparrow}d_{B\uparrow}d_{A\downarrow}). \end{aligned}$$

The original onsite Coulomb repulsion is resolved into complex charging processes of many types: (i) intralevel, (ii) interlevel, (iii) two-electron transfer, and (iv) two-electron exchange interactions. Interactions (i) and (ii) refer to electrons with different spins in the same state and in two states, respectively. Interaction (iii) is the simultaneous transfer of electrons between molecular states. These two terms can be written in a form that is consistent with the physical picture presented herein, in which interlevel electron transfer can occur only via the spin-flip coupling. The negative sign in each term follows from the time-reversal invariance, consistent with Eq. (21). Interaction (iv) is the interlevel two-electron exchange process during which the electron spins are preserved. It is inconsistent with the interpretation herein, in which direct interlevel hopping is prohibited. Furthermore, the rearranging of these two terms into the intralevel spin-flip form is not physically reasonable. In summary, interactions (i)–(iii) are compatible with the presented interpretation, and components in interaction (iii) are arranged in a form that can be interpreted as spin-flip charging process, while those in interaction (iv), associated with direct hopping, are not.

APPENDIX B

The spin-resolved linear conductance is derived using the Green's function technique. All functions are written in the space $L \otimes S$, defined by the Kronecker product

$$L \otimes S = \begin{pmatrix} L_{11}S & L_{12}S \\ L_{21}S & L_{22}S \end{pmatrix},$$

where L represents the orbital state, and S represents the spin. Based on Eqs. (20)–(22), the bare Green's function for isolated SQDM and the level-width functions are given by matrices in the molecular basis,

$$[\mathbf{g}^r(\omega)]^{-1} = \begin{pmatrix} \omega-\varepsilon+t_{d_1d_2} & 0 & 0 & t^{R*}_{d_1d_2} \\ 0 & \omega-\varepsilon-t_{d_1d_2} & -t^{R*}_{d_1d_2} & 0 \\ 0 & -t^{R}_{d_1d_2} & \omega-\varepsilon+t_{d_1d_2} & 0 \\ t^{R}_{d_1d_2} & 0 & 0 & \omega-\varepsilon-t_{d_1d_2} \end{pmatrix};$$

$$\Gamma^{\alpha=L,R}(\omega) = \begin{pmatrix} \gamma^\alpha_B(\omega) & \sqrt{\gamma^\alpha_B(\omega)\gamma^\alpha_A(\omega)} & 0 & 0 \\ \sqrt{\gamma^\alpha_B(\omega)\gamma^\alpha_A(\omega)} & \gamma^\alpha_A(\omega) & 0 & 0 \\ 0 & 0 & \gamma^\alpha_B(\omega) & \sqrt{\gamma^\alpha_B(\omega)\gamma^\alpha_A(\omega)} \\ 0 & 0 & \sqrt{\gamma^\alpha_B(\omega)\gamma^\alpha_A(\omega)} & \gamma^\alpha_A(\omega) \end{pmatrix}, \tag{B1}$$

where the symmetric phase condition $\phi_1 = \phi_2$ is considered, and $\Gamma^\alpha(\omega)$ describes the coupling of lead α to the SQDM,

$$\Gamma^{L(R)}_{ij\sigma}(\omega) \equiv 2\pi \sum_{k\in L(R)} t_{L(R)d_i\sigma} t^*_{L(R)d_j\sigma} \delta(\omega - \varepsilon_{L(R)k}),$$

with $\Gamma^\alpha_{BB\sigma}(\omega) \equiv \gamma^\alpha_B(\omega)$, $\Gamma^\alpha_{AA\sigma}(\omega) \equiv \gamma^\alpha_A(\omega)$, and $\Gamma^\alpha_{BA\sigma}(\omega) = \Gamma^\alpha_{AB\sigma}(\omega) \equiv \sqrt{\gamma^\alpha_B(\omega)\gamma^\alpha_A(\omega)}$. Generally, the spin-dependent phases that result from spin precession differ. The diagonal matrix elements are as follows:

$$\begin{aligned}
\gamma^L_B &\propto t_{Ld_B} t^*_{Ld_B} = \tfrac{1}{2}\left(t_{Ld_1} - t_{Ld_2}\right)^2,\\
\gamma^L_A &\propto t_{Ld_A} t^*_{Ld_A} = \tfrac{1}{2}\left(t_{Ld_1} + t_{Ld_2}\right)^2;\\
\gamma^R_{B\sigma} &\propto t_{Rd_B\sigma} t^*_{Rd_B\sigma} = \tfrac{1}{2}\left(t^2_{Rd_1} - t_{Rd_1} t_{Rd_2} e^{-i\sigma(\phi_1-\phi_2)}\right.\\
&\quad \left. - t_{Rd_1} t_{Rd_2} e^{i\sigma(\phi_1-\phi_2)} + t^2_{Rd_2}\right),\\
\gamma^R_{A\sigma} &\propto t_{Rd_A\sigma} t^*_{Rd_A\sigma} = \tfrac{1}{2}\left(t^2_{Rd_1} + t_{Rd_1} t_{Rd_2} e^{-i\sigma(\phi_1-\phi_2)}\right.\\
&\quad \left. + t_{Rd_1} t_{Rd_2} e^{i\sigma(\phi_1-\phi_2)} + t^2_{Rd_2}\right).
\end{aligned}$$

Many features can be summarized: (i) $t_{\alpha d_B\sigma} \neq t_{\alpha d_A\sigma} \Rightarrow \gamma^\alpha_{B\sigma} \neq \gamma^\alpha_{A\sigma}$, (ii) $\phi_1 = \phi_2 \equiv \phi \Rightarrow \gamma^R_{B(A)\uparrow} = \gamma^R_{B(A)\downarrow} \equiv \gamma^R_{B(A)}$, indicating that the couplings of the molecular states to the right lead also become spin independent, and (iii) $t_{\alpha d_1} = t_{\alpha d_2} \Rightarrow \gamma^\alpha_B = 0$. Notably, the off-diagonal components characterize either point-like propagation through reservoir $\sqrt{\gamma^\alpha_B(\omega)\gamma^\alpha_A(\omega)} \equiv \gamma^\alpha(\omega)$ or individual reservoirs $\sqrt{\gamma^\alpha_B(\omega)\gamma^\alpha_A(\omega)} = 0$, corresponding to the physical pictures of ideal indirect coupling between two dots and electron transfer between dots, restricted by direct coupling, respectively. Furthermore, in the limit of a linear response, only functions at the Fermi level are involved in the conductance formula. In a self-energy matrix, the effects of the charge source and drain are written as

$$\Sigma^r(\mu) = -\frac{i}{2}[\Gamma^L(\mu) + \Gamma^R(\mu)] = -i\begin{pmatrix} \gamma_B & \gamma & 0 & 0\\ \gamma & \gamma_A & 0 & 0\\ 0 & 0 & \gamma_B & \gamma\\ 0 & 0 & \gamma & \gamma_A \end{pmatrix}, \tag{B2}$$

where, for simplicity, the symmetric condition $\gamma^L_B(\mu) = \gamma^R_B(\mu) \equiv \gamma_B$, $\gamma^L_A(\mu) = \gamma^R_A(\mu) \equiv \gamma_A$, and $\gamma^L(\mu) = \gamma^R(\mu) \equiv \gamma$ is considered. Based on Eqs. (B1) and (B2), the full retarded Green's function is obtained by applying the Dyson equation

$$\begin{aligned}
\mathbf{G}^r(\mu) &= \mathbf{g}^r(\mu) + \mathbf{g}^r(\mu)\Sigma^r(\mu)\mathbf{G}^r(\mu) = [\mu\mathbf{I} - \mathbf{H} - \Sigma^r(\mu)]^{-1}\\
&= \begin{pmatrix} \mu - \varepsilon + t_{d_1d_2} + i\gamma_B & i\gamma & 0 & t^{R*}_{d_1d_2}\\ i\gamma & \mu - \varepsilon - t_{d_1d_2} + i\gamma_A & -t^{R*}_{d_1d_2} & 0\\ 0 & -t^R_{d_1d_2} & \mu - \varepsilon + t_{d_1d_2} + i\gamma_B & i\gamma\\ t^R_{d_1d_2} & 0 & i\gamma & \mu - \varepsilon - t_{d_1d_2} + i\gamma_A \end{pmatrix}^{-1}.
\end{aligned}$$

Specifying the bare level position ε with respect to the Fermi level of the leads yields the total transmission

$$\begin{aligned}
T(\varepsilon) &= \mathrm{Tr}[\mathbf{G}^r(\varepsilon)\Gamma^L(\varepsilon)\mathbf{G}^a(\varepsilon)\Gamma^R(\varepsilon)]\\
&= 2\frac{2\left(\varepsilon^2 - t^2_{d_1d_2} - \left|t^R_{d_1d_2}\right|^2 + \gamma^2 - 2\gamma_B\gamma_A\right)\gamma^2 + \left(\varepsilon + t_{d_1d_2}\right)^2\gamma^2_B + (\varepsilon - t_{d_1d_2})^2\gamma^2_A + 2\gamma^2_B\gamma^2_A + 2\left|t^R_{d_1d_2}\right|^2\gamma_B\gamma_A}{\left[\varepsilon^2 - \left(t^2_{d_1d_2} + \left|t^R_{d_1d_2}\right|^2 - \gamma^2\right)\right]^2 + \left(\varepsilon + t_{d_1d_2}\right)^2\gamma^2_B + \left(\varepsilon - t_{d_1d_2}\right)^2\gamma^2_A + \gamma^2_B\gamma^2_A + 2\left|t^R_{d_1d_2}\right|^2\gamma_B\gamma_A - 2\gamma^2\gamma_B\gamma_A}.
\end{aligned}$$

Consider now the fully symmetric case $t_{\alpha d_1} = t_{\alpha d_2}$, leading to $\gamma^\alpha_B = \gamma = 0$: a Lorentzian-type resonant transmission is given by

$$T(\varepsilon) = 2\frac{\left(\varepsilon - t_{d_1d_2}\right)^2\gamma^2_A}{\left[\varepsilon^2 - \left(t^2_{d_1d_2} + \left|t^R_{d_1d_2}\right|^2\right)\right]^2 + \left(\varepsilon - t_{d_1d_2}\right)^2\gamma^2_A}. \tag{B3}$$

Notably, Eq. (B3) specifies the energy-dependent level width. The linear conductance curve comprises two resonances, with the following corresponding peak positions and level widths:

$$\begin{aligned}
&\varepsilon = \sqrt{t^2_{d_1d_2} + |t^R_{d_1d_2}|^2}, \quad \Gamma = \left(\sqrt{t^2_{d_1d_2} + |t^R_{d_1d_2}|^2} - t_{d_1d_2}\right)^2\gamma^2_A;\\
&\varepsilon = -\sqrt{t^2_{d_1d_2} + |t^R_{d_1d_2}|^2}, \quad \Gamma = \left(-\sqrt{t^2_{d_1d_2} + |t^R_{d_1d_2}|^2} - t_{d_1d_2}\right)^2\gamma^2_A.
\end{aligned}$$

The expression for the bonding level width clearly reveals that the bonding resonance emerges because of the transverse RSO component. In contrast, the bonding state becomes a BIC when $t^R_{d_1d_2} = 0$, owing to the zero level width. The lifetime of the bonding state clearly exceeds that of the antibonding state by comparing the inverse level width. Therefore, the evolution of the narrower peak, revealed by the above transmission, is completely consistent with the physical picture and NEGF results that are presented in Sec. III. Additionally, Fano resonance[38] that arises from the interference between molecular states with different level widths is also demonstrated. Given by the imaginary parts of the diagonal Green's functions, the densities of the bonding and antibonding states are

$$\rho_B(\varepsilon) = \frac{1}{\pi}\frac{2\left|t^R_{d_1d_2}\right|^2\gamma_A}{\left[\varepsilon^2 - \left(t^2_{d_1d_2} + \left|t^R_{d_1d_2}\right|^2\right)\right]^2 + \left(\varepsilon - t_{d_1d_2}\right)^2\gamma^2_A}$$

and

$$\rho_A(\varepsilon) = \frac{1}{\pi}\frac{2\left(\varepsilon - t_{d_1d_2}\right)^2\gamma_A}{\left[\varepsilon^2 - \left(t^2_{d_1d_2} + \left|t^R_{d_1d_2}\right|^2\right)\right]^2 + \left(\varepsilon - t_{d_1d_2}\right)^2\gamma^2_A}.$$

*d93222013@ntu.edu.tw
†crchang@phys.ntu.edu.tw

[1]C. Wu and S.-C. Zhang, Phys. Rev. Lett. **93**, 036403 (2004).
[2]V. K. Dugaev, M. Inglot, E. Y. Sherman, J. Berakdar, and J. Barnas, Phys. Rev. Lett. **109**, 206601 (2012).
[3]S. Nakosai, Y. Tanaka, and N. Nagaosa, Phys. Rev. Lett. **108**, 147003 (2012).
[4]J. Nitta, T. Akazaki, H. Takayanagi, and T. Enoki, Phys. Rev. Lett. **78**, 1335 (1997).
[5]E. Eriksson, A. Strom, G. Sharma, and H. Johannesson, Phys. Rev. B **86**, 161103(R) (2012).
[6]L. A. Gonzalez-Arraga, B. Berche, and E. Medina, Phys. Rev. B **86**, 155312 (2012).
[7]Q.-F. Sun and X. C. Xie, Phys. Rev. B **73**, 235301 (2006).
[8]D. Sanchez and L. Serra, Phys. Rev. B **74**, 153313 (2006).
[9]A. M. Lobos and A. A. Aligia, Phys. Rev. Lett. **100**, 016803 (2008).
[10]C. Flindt, A. S. Sorensen, and K. Flensberg, Phys. Rev. Lett. **97**, 240501 (2006).
[11]M. Borhani and X. Hu, Phys. Rev. B **85**, 125132 (2012).
[12]H. L. Calvo, L. Classen, J. Splettstoesser, and M. R. Wegewijs, Phys. Rev. B **86**, 245308 (2012).
[13]D. Loss and D. P. DiVincenzo, Phys. Rev. A **57**, 120 (1998).
[14]S. Goswami, M. A. Aamir, C. Siegert, M. Pepper, I. Farrer, D. A. Ritchie, and A. Ghosh, Phys. Rev. B **85**, 075427 (2012).
[15]M. Sigrist, T. Ihn, K. Ensslin, M. Reinwald, and W. Wegscheider, Phys. Rev. Lett. **98**, 036805 (2007).
[16]V. Puller, Y. Meir, M. Sigrist, K. Ensslin, and T. Ihn, Phys. Rev. B **80**, 035416 (2009).
[17]A. C. Johnson, C. M. Marcus, M. P. Hanson, and A. C. Gossard, Phys. Rev. Lett. **93**, 106803 (2004).
[18]M. L. Ladron de Guevara, F. Claro, and P. A. Orellana, Phys. Rev. B **67**, 195335 (2003).
[19]F. H. Stillinger and D. R. Herrick, Phys. Rev. A **11**, 446 (1975).
[20]J. V. Neumann and E. Wigner, Phys. Z. **30**, 465 (1929).
[21]H. Friedrich and D. Wintgen, Phys. Rev. A **31**, 3964 (1985).
[22]F. Chi, J.-L. Liu, and L.-L. Sun, J. Appl. Phys. **101**, 093704 (2007).
[23]H.-T. Yin, X.-J. Liu, L.-F. Feng, T.-Q. Lu, and H. Li, Phys. Lett. A **374**, 2865 (2010).
[24]F. Chi, X. Yuan, and J. Zheng, Nanoscale Research Letters **3**, 343 (2008).
[25]Q.-F. Sun, J. Wang, and H. Guo, Phys. Rev. B **71**, 165310 (2005).
[26]X. Hu and S. Das Sarma, Phys. Rev. A **61**, 062301 (2000).
[27]D. S. Duncan, C. Livermore, R. M. Westervelt, K. D. Maranowski, and A. C. Gossard, Appl. Phys. Lett. **74**, 1045 (1999).
[28]L. V. Keldysh, Zh. Eksp. Teor. Fiz. **47**, 1515 (1964) [Sov. Phys.–JETP **20**, 1018 (1965)].
[29]T. Ihn, M. Sigrist, K. Ensslin, W. Wegscheider, and M. Reinwald, New J. Phys. **9**, 111 (2007).
[30]Y. Meir and N. S. Wingreen, Phys. Rev. Lett. **68**, 2512 (1992).
[31]G. D. Mahan, *Many-Particle Physics*, 3rd ed. (Springer, Berlin, 2000).
[32]A. Groshev, T. Ivanov, and V. Valtchinov, Phys. Rev. Lett. **66**, 1082 (1991).
[33]G. Schedelbeck, W. Wegscheider, M. Bichler, and G. Abstreiter, Science **278**, 1792 (1997).
[34]K.-W. Chen and C.-R. Chang, Phys. Rev. B **78**, 235319 (2008).
[35]A. Silva, Y. Oreg, and Y. Gefen, Phys. Rev. B **66**, 195316 (2002).
[36]M. L. Ladron de Guevara and P. A. Orellana, Phys. Rev. B **73**, 205303 (2006).
[37]K.-W. Chen, M.-H. Liu, S.-H. Chen, and C.-R. Chang, IEEE Trans. Magn. **43**, 2866 (2007).
[38]U. Fano, Phys. Rev. **124**, 1866 (1961).